1992

A Mathematical Model of a CuO/Cu Vaporvolt Cell

Makoto Kawanami
Texas A & M University - College Station

Trung V. Nguyen
Texas A & M University - College Station

Ralph E. White
University of South Carolina - Columbia, white@cec.sc.edu

Publication Info

Journal of the Electrochemical Society, 1992, pages 3408-3415.

Publisher's link: http://dx.doi.org/10.1149/1.2069092
DOI: 10.1149/1.2069092

since polymerization rate of the conducting polymers affects the polymer morphology.[19] Actually, the polymerization current of c-PTE was found to be about one-fifth of t-PTE, again suggesting restricted polymerization kinetics in the polymerization of the *cis*-monomer.

The longevity of c-PTE was also investigated under a constant current of 0.05 mA. As shown in Fig. 9, the coulombic efficiency was stable over 100 cycles, while the discharge capacity decreased after about 100 cycles. The origin of the limited longevity is not thought to be intrinsic, but extrinsic. That is, the polymer film may peel off from the ITO substrate during repetitive charge-discharge cycles. Since the volume of conducting polymers is known to change with doping and undoping, the volume change during the doping-undoping cycle is thought to be one of the causes of the peel off phenomenon.[20]

Summary

1. Electrochemical characteristics of PTEs which were prepared from *trans*- and *cis*-monomers were investigated in TBAFB/NB and $LiBF_4$/PC solution.

2. Same doping-undoping potentials and electrochemical reversibilities were observed in t-PTE and c-PTE.

3. T-PTE and c-PTE showed excellent characteristics for use as electrode active materials in rechargeable batteries such as fairly stable charge-discharge potentials, nearly 100% of coulombic efficiency, and capability for high rate charge-discharge cycles with relatively large charge-discharge current.

4. Relatively high doping ratio was observed in the nitrobenzene solution resulting in high discharge capacity of c-PTE.

5. The higher doping ratio and, thus, higher discharge capacity in c-PTE compared to those in t-PTE was observed and was explained in term of the higher apparent diffusion coefficient of dopant ion (BF_4^-) within c-PTE than t-PTE.

Manuscript submitted Oct. 14, 1991; revised manuscript received July 29, 1992.

REFERENCES

1. E. S. Su, J. R. Schrieffer, and A. J. Heeger, *Phys. Rev. Lett.*, **42,** 1698 (1979).
2. S. N. Chen, A. J. Heeger, Z. Kiss, A. G. MacDiarmid, S. C. Gu, and D. L. Peebles, *Appl. Phys. Lett.*, **36,** 96 (1980).
3. J. C. Scott, P. Pfluger, M. T. Krounbi, and G. B. Street, *Phys. Rev.*, **28,** 2140 (1983).
4. T. Kawai, T. Kuwabara, S. Wang, and K. Yoshino, *Jpn. J. Appl. Phys.*, **29,** 602 (1990).
6. T. Kawai, T. Kuwabara, S. Wang, and K. Yoshino, *This Journal*, **137,** 3793 (1990).
7. Y. Ohmori, H. Takahashi, K. Muro, M. Uchida, T. Kawai, and K. Yoshino, *Jpn. J. Appl. Phys.*, **30,** L601 (1991).
8. J. H. Burroughes, D. D. C. Bradley, A. R. Brown, R. N. Marks, K. Mackay, R. H. Friend, P. L. Burns, and A. B. Holmes, *Nature*, **347,** 539 (1990).
9. D. Braun and A. J. Heeger, *Appl. Phys. Lett.*, **58,** 1982 (1991).
10. Y. Ohmori, M. Uchida, K. Muro, and K. Yoshino, *Solid State Commun.*, **80,** 605 (1991).
11. R. Sugimoto, S. Takeda, H. B. Gu, and K. Yoshino, *Chem. Express*, **1,** 635 (1986).
12. I. Murase, T. Ohnishi, T. Noguchi, and M. Hirooka, *Polym. Commun.*, **28,** 229 (1987).
13. M. Onoda, S. Morita, T. Iwasa, H. Nakayama, and K. Yoshino, *J. Chem. Phys.*, **95,** 8584 (1991).
14. M. Onoda, T. Iwasa, T. Kawai, and K. Ysohino, *J. Phys. D: Appl. Phys.*, **24,** 2076 (1991).
15. M. Onoda, T. Iwasa, T. Kawai, and K. Yoshino, *J. Phys. Soc. Jpn.*, **60,** 3768 (1991).
16. K. Yoshino, T. Kuwabara, and T. Kawai, *Jpn. J. Appl. Phys.*, **29,** L995 (1990).
17. K. Yoshino, T. Kuwabara, T. Iwasa, T. Kwai, and M. Onoda, *Chem. Express*, **5,** 325 (1990).
18. R. W. Murray, in *Electroanalytical Chemistry*, Vol. 13, A. J. Bard, Editor, p. 191, Marcel Dekker, Inc., New York (1984).
19. S. Kuwabata, K. Okamoto, and H. Yoneyama, *J. Chem. Soc., Faraday Trans. 1*, **84,** 2317 (1988).
20. T. Kawai, M. Nakazono, and K. Yoshino, *J. Mat. Chem.*, **2,** 903 (1992).

A Mathematical Model of a CuO/Cu Vaporvolt Cell

Makoto Kawanami,* Trung V. Nguyen,,[a] and Ralph E. White****

Department of Chemical Engineering, Texas A&M University, College Station, Texas 77843-3122

ABSTRACT

A new battery named "Vaporvolt"[b] cell is in the early stage of its development. A mathematical model of a CuO/Cu Vaporvolt cell is presented that can be used to predict the potential and the transport behavior of the cell during discharge. A sensitivity analysis of the various transport and electrokinetic parameters indicates which parameters have the most influence on the predicted energy and power density of the Vaporvolt cell. This information can be used to decide which parameters should be optimized or determined more accurately through further modeling or experimental studies. The optimal thicknesses of electrodes and separator, the concentration of the electrolyte, and the current density are determined by maximizing the power density. These parameter sensitivities and optimal design parameter values help in the development of a better CuO/Cu Vaporvolt cell.

Batteries with higher energy and power densities have been desired for years. The traditional approach has been to employ more energetic reactions, which result in higher unit cell voltage, to achieve higher power and energy densities.[1-13] Although both stored energy and power densities have increased by this approach,[14] specific stored energy and power densities are still relatively low. This is because of the additional weight required to contain these highly reactive materials and to maintain the mechanical strength of the battery. In addition, the energy densities of secondary batteries are much lower than that of primary batteries.[15] Furthermore, there is a safety concern associated with using highly reactive chemicals such as lithium and thionyl chloride.[16-18] Another approach for achieving higher specific energy and power densities is to minimize unnecessary weight and volume in existing systems.

Vaporvolt cells, which currently are being evaluated by Energy Innovations, Inc., for NASA as possible replacements for higher power density primary lithium batteries, use this approach. Weight and volume are minimized by

* Electrochemical Society Student Member.
** Electrochemical Society Active Member.
[a] Present address: AT&T Bell Laboratories, Mesquite, TX 75149.

using thin laminations of metals and their oxides as the active materials of a battery.[19] Reaction rates at the electrode surfaces of these batteries are low, resulting in minimal stress on the electrodes. High currents are obtained by using the high area per volume characteristic of thin laminations. Desired voltage can be obtained by bipolar construction. Electrochemical conversion is accomplished by displacing oxygen from one metal to the other. There are no side reactions that complicate the process and make unwanted by-products; and, in most cases, the energy conversion process is highly reversible.

In designing high performance Vaporvolt cells, there are various attributes that can influence the system significantly. Such attributes might be the thicknesses of the electrodes and the separator, KOH concentration, and the current density. A sensitivity analysis is performed on various parameters to determine which parameters are most influential in increasing or decreasing the energy and power densities. This information can indicate the direction one should take to design better Vaporvolt cells. The results of the sensitivity analysis also can suggest which parameters should be obtained with more accuracy through further modeling studies or experimentation.

To achieve high performance in the Vaporvolt cell, various design parameters can be optimized so that the cell delivers the maximum attainable power density. The important parameters in the Vaporvolt cell are the thicknesses of the positive electrode (L_{pos}), negative electrode (L_{neg}) and separator (L_s), the concentration of KOH (c_{KOH}), and current density (i). The CuO/Cu system was selected in this investigation because the CuO/Cu Vaporvolt cells are the only successfully manufactured batteries at this time. By using a mathematical model of the CuO/Cu Vaporvolt cell, these parameters are investigated to determine if an optimal value exists for each parameter. The sensitivity of the model predictions to various parameters are then examined followed by determination of the optimal design parameters to maximize the power density of the Vaporvolt cell.

Model Development

The reactions occurring in the CuO/Cu Vaporvolt cell during discharge are the reduction of CuO at the cathode (positive electrode)

$$\text{Positive Electrode: } CuO + \frac{1}{2}H_2O + e^- \rightarrow \frac{1}{2}Cu_2O + OH^- \quad [1]$$

and the oxidation of copper at the anode (negative electrode)

$$\text{Negative Electrode: } Cu + OH^- \rightarrow \frac{1}{2}Cu_2O + \frac{1}{2}H_2O + e^- \quad [2]$$

The overall reaction is the production of Cu_2O from CuO and Cu

$$\text{Total: } CuO + Cu \rightarrow Cu_2O \quad [3]$$

Since the solubility of Cu_2O in basic solution is very low, solid Cu_2O is formed during discharge. The open-circuit voltage of a CuO/Cu Vaporvolt cell is 198 mV, based on the electrochemical data at 25°C.[20] This open-circuit voltage of CuO/Cu couple is not high. If we employ a system with higher open-circuit voltage, we can obtain higher energy and power density. However; the CuO/Cu couple is the only successfully manufactured Vaporvolt cell at this time.

The objective of the present investigation is to develop a mathematical model that can be used to estimate the optimum values of transport and electrokinetic parameters, and to predict the maximum attainable energy and power densities of a CuO/Cu Vaporvolt cell.

The assumptions are as follows.

1. A one-dimensional model can describe the behavior of the cell.

2. Dilute solution theory[21] applies. To avoid the complexities associated with using concentrated solution theory, we decided to use dilute solution theory. If better prediction is needed we account for the species interactions by using diffusion coefficients that are obtained experimentally. Negligible interactions between the solutes are assumed.

3. The Nernst-Einstein equation, $D_i = u_i RT$, which is implicit in the dilute solution theory, applies.

4. The current density takes the form of the Butler-Volmer equation, which expresses the exponential dependence of the current on the overpotential.

5. The physical, transport, and electrokinetic parameters are constant throughout the solution.

6. The cell is isothermal.

7. No homogeneous chemical reactions occur in the electrolyte.

8. There is no electrolyte movement.

9. The electrochemical reactions occur at the surface of the electrodes.

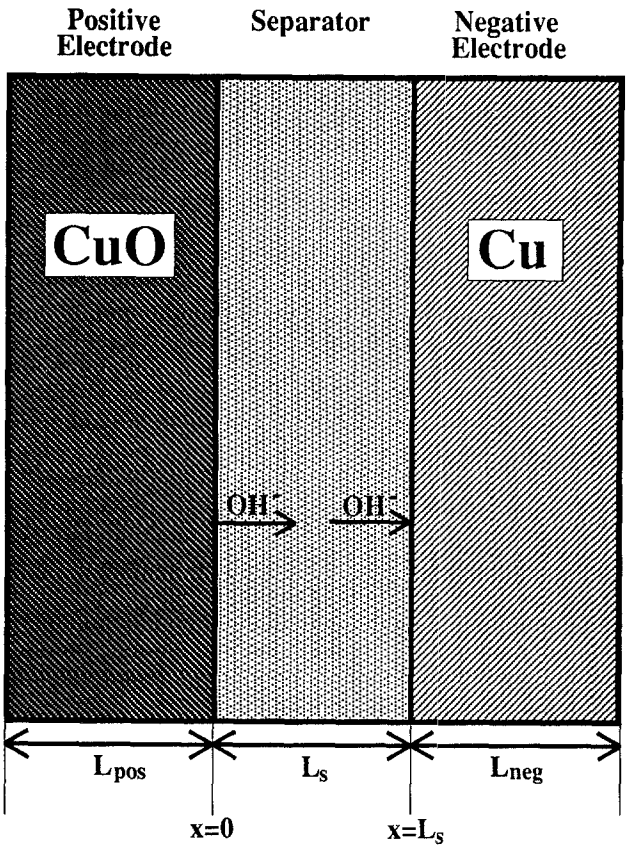

Fig. 1. Schematic of a Vaporvolt cell.

A schematic of a CuO/Cu Vaporvolt cell is shown in Fig. 1. During discharge of a CuO/Cu Vaporvolt cell, hydroxide ions are released from the positive electrode (Eq. 1), and consumed at the negative electrode (Eq. 2). Therefore, hydroxide ions must be transported in the electrolyte in the separator from the positive electrode to the negative electrode. Mass transport in this system is due to migration in an electric field and diffusion in a concentration gradient. Therefore, the flux expression for each species i can be written as

$$\mathbf{N}_i = -z_i u_i F c_i \nabla\Phi - D_i \nabla c_i \quad [4]$$

where the ionic mobility, u_i, is assumed to be related to the diffusion coefficient D_i by the Nernst-Einstein equation

$$u_i = \frac{D_i}{RT} \quad [5]$$

The differential material balance equation for each species without homogeneous chemical reactions in the electrolyte is

$$\frac{\partial c_i}{\partial t} = -\nabla \cdot \mathbf{N}_i \quad [6]$$

By combining Eq. 4 and 6, we can obtain the following equation

$$\frac{\partial c_i}{\partial t} = z_i u_i F(c_i \nabla^2 \Phi + \nabla c_i \cdot \nabla \Phi) + D_i \nabla^2 c_i \quad [7]$$

Since the net charge in the bulk electrolyte is zero, the equation of electroneutrality

$$\sum_i z_i c_i = 0 \quad [8]$$

must hold in the electrolyte. The flow of charge is related to the current density **i** in the solution

$$\mathbf{i} = F \sum_i z_i \mathbf{N}_i \quad [9]$$

Equations 4 and 9 can be combined and rearranged to get

$$\nabla \Phi = \frac{-\mathbf{i}}{\kappa} - \frac{F}{\kappa}\left(\sum_i z_i D_i \nabla c_i\right) \quad [10]$$

where

$$\kappa = \frac{F^2}{RT} \sum_i z_i^2 D_i c_i \quad [11]$$

Equations 7 and 10 for one spatial coordinate reduce to Eq. 12 and 13, respectively

$$\frac{\partial c_i}{\partial t} = z_i u_i F \left(c_i \frac{\partial^2 \Phi}{\partial x^2} + \frac{\partial c_i}{\partial x}\frac{\partial \Phi}{\partial x}\right) + D_i \frac{\partial^2 c_i}{\partial x^2} \quad [12]$$

$$\frac{\partial \Phi}{\partial x} = \frac{-i}{\kappa} - \frac{F}{\kappa}\left(\sum_i z_i D_i \frac{\partial c_i}{\partial x}\right) \quad [13]$$

There are three unknowns c_{K^+}, c_{OH^-}, and Φ, so we need three governing equations. Equation 8 is used for c_{K^+}, Eq. 12 is used for c_{OH^-}, and Eq. 13 is used for Φ.

The initial and the boundary conditions for these dependent variables are as follows: at $t = 0$, the concentration of the species are their initial values

$$\text{For all } x \text{ at } t = 0 \qquad c_i(t = 0, x) = c_i^\circ \quad [14]$$

since c_i° must obey $\Sigma_i z_i c_i^\circ = 0$.

At $x = 0$, (positive electrode surface), the change in the concentration of OH^- is related to the current density since the number of OH^- ions released at the positive electrode surface is proportional to the number of the electrons received at the electrode, that is, current density (Eq. 1)

$$\text{For all } t,\ t > 0 \quad \left.\frac{\partial c_{OH^-}}{\partial x}\right|_{x=0} = \frac{i}{n_1 F D_{OH^-}} \quad [15]$$

where n_1 is the number of electrons transferred in Eq. 1.

At $x = L_s$ (negative electrode surface), the change in the concentration of OH^- also is related to the current density (Eq. 2)

$$\text{For all } t,\ t > 0 \quad \left.\frac{\partial c_{OH^-}}{\partial x}\right|_{x=L_s} = \frac{i}{n_2 F D_{OH^-}} \quad [16]$$

where n_2 is the number of electrons transferred in Eq. 2.

Since we cannot measure the absolute potential, we need to fix a potential at $x = 0$

$$\text{For all } t \text{ at } x = 0 \qquad \Phi(t, x = 0) = 0 \quad [17]$$

The relation between the current density, i, and the overpotential, η, is expressed by the Butler-Volmer electrochemical rate expression

$$i = i^\circ \frac{A^*}{A}\left[\prod_i \left(\frac{c_i}{c_i^r}\right)^{p_i} \exp\left(\frac{\alpha_a F}{RT}\eta\right) - \prod_i \left(\frac{c_i}{c_i^r}\right)^{q_i} \exp\left(\frac{-\alpha_c F}{RT}\eta\right)\right] \quad [18]$$

where A^* and A are the active surface area of the electrode and the geometric surface area of the electrode, respectively. Active surface area of the electrodes decreases with the discharge of the cell since Cu_2O, that has low electric conductivity, is formed on the electrodes during discharge. The active surface area of each electrode is assumed to change according to the following equation

$$A^* = A \frac{m}{m^\circ} \quad [19]$$

where m is the amount of active material (CuO for positive electrode, Cu for negative electrode) in an electrode at time t, and m° is the initial amount of active material in the electrode. m° is simply expressed by the following equation

$$m^\circ = L_j d_j \quad [20]$$

where L_j is the thickness of the electrode and d_j is the density of the electrode. For a constant current density discharge, m changes with time according to following equation

$$m = m^\circ - \frac{M_j i t}{n_j F} \quad [21]$$

where M_j is a molecular weight of an electrode j.

By combining Eq. 18 through 21, we can obtain the following relation between the current density i and the overpotential η

$$i = i^\circ \left(1 - \frac{M_j i t}{L_j d_j n_j F}\right)\left[\prod_i \left(\frac{c_i}{c_i^r}\right)^{p_i} \exp\left(\frac{\alpha_a F}{RT}\eta\right) - \prod_i \left(\frac{c_i}{c_i^r}\right)^{q_i} \exp\left(\frac{-\alpha_c F}{RT}\eta\right)\right] \quad [22]$$

Note that CuO, Cu_2O, and Cu exist as solids because of their low solubility in a basic solution, so the values of $(c_i/c_i^r)^{p_i}$ and $(c_i/c_i^r)^{q_i}$ for CuO, Cu_2O, and Cu in Eq. 22 remain constant. In addition, the anodic and cathodic transfer coefficients are assumed to sum to the number of electrons transferred (*i.e.*, $\alpha_a + \alpha_c = n_j$), and the reaction order coefficients are assumed to be simply related to s_i

$$\begin{aligned} p_i &= s_i \quad q_i = 0 \quad \text{if } s_i > 0 \\ p_i &= 0 \quad q_i = -s_i \quad \text{if } s_i < 0 \end{aligned} \quad [23]$$

And the electrode potentials, E_{pos} and E_{neg}, are expressed by

$$E_{pos} = U_{pos} + \Phi(t, x = 0) + \eta_{pos} \quad [24]$$

$$E_{neg} = U_{neg} + \Phi(t, x = L_s) + \eta_{neg} \quad [25]$$

where U_{pos} and U_{neg} are the open-circuit potentials of the positive and negative electrodes, respectively.

The potential of a Vaporvolt cell, E_{cell}, is the difference between the potentials of the positive electrode and the negative electrode. By subtracting Eq. 25 from Eq. 24

$$\begin{aligned} E_{cell} &= E_{pos} - E_{neg} \\ &= U_{cell} - \Phi(t, x = L_s) + \eta_{pos} - \eta_{neg} \end{aligned} \quad [26]$$

$$U_{cell} = U_{pos} - U_{neg} \quad [27]$$

where U_{cell} is the open-circuit potential of the Vaporvolt cell.

Note that an overpotential takes a negative value at the positive electrode, and takes a positive value at the negative electrode, and $\Phi(t, x = L_s)$ is always positive during discharge because negatively charged particles (OH^-) must transport from the positive electrode ($x = 0$) to the negative electrode ($x = L_s$). Therefore, the potential of a Vaporvolt cell, E_{cell}, is always smaller than the open-circuit potential of the Vaporvolt cell, U_{cell}.

Equations 4-13 represent the basic governing equations necessary to describe the behavior in the electrolyte of a Vaporvolt cell. These equations are solved numerically by setting the cell current density, i, and calculating the potential of the Vaporvolt cell, E_{cell}, or the power density, P (=iE_{cell}). BAND(J), a finite difference numerical technique developed by Newman,[21] was used to solve the equations. The model parameters associated with these equations are shown in Table I.

Table I. Base case parameter values for the CuO/Cu Vaporvolt cell simulation.

Structural parameters	
Thickness of positive electrode (CuO) (L_{pos})	0.00254 cm
Thickness of negative electrode (Cu) (L_{neg})	0.00254 cm
Separator thickness (L_s)	0.00254 cm
Open-circuit potential (U_{cell})	198 mV
Current density (i)	0.001 A/cm^2
Anodic and cathodic exchange current densities (i^o)	0.001 A/cm^2
Anodic transfer coefficient for Cu oxidation ($\alpha_{a,Cu}$)	0.5
Cathodic transfer coefficient for CuO reduction ($\alpha_{c,CuO}$)	0.5
Electrolyte concentration (c_{KOH})	8.3878M
Initial K^+ concentration ($c^o_{K^+}$)	8.3878M
Initial OH^- concentration ($c^o_{OH^-}$)	8.3878M
Reference K^+ concentration ($c^r_{K^+}$)	1.0000M
Reference OH^- concentration ($c^r_{OH^-}$)	1.0000M
Temperature (T)	298 K

Table II. Comparison of performances of Vaporvolt cells with different separator thicknesses.

Separator thickness	0.00254 cm	0.00508 cm
Cell capacity	17.82711 C/cm^2	17.82711 C/cm^2
Energy density	1.88573 Ws/cm^2	1.88569 Ws/cm^2
Power density	0.10637 mW/cm^2	0.10636 mW/cm^2

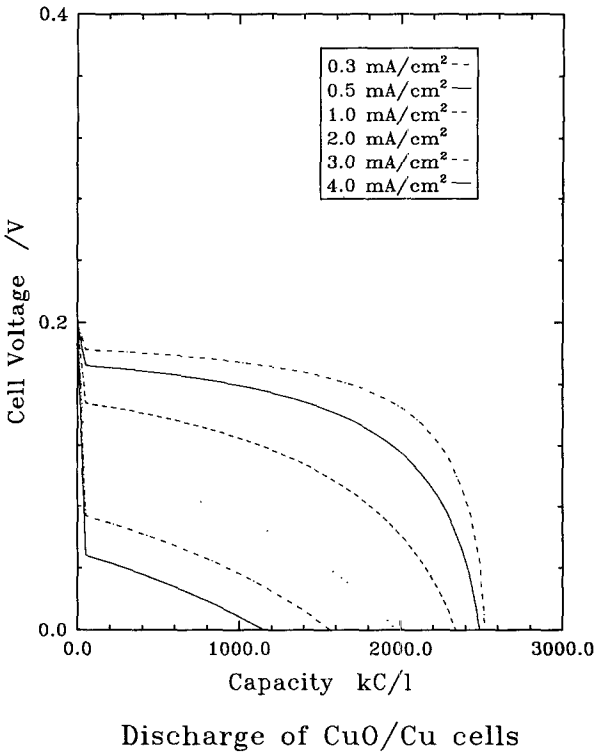

Fig. 2. Cell voltage *vs.* capacity delivered.

Results and Discussion

Although we assume that the electrochemical reaction occurs only at the surface of the active material, the reaction layer moves to the inside of the active material as the cell discharges. Therefore, the thickness of the mass transport region of the cell increases as the cell discharges. To check the validity of this assumption, the cell performances with different separator thicknesses are predicted and compared. First, the cell performance is predicted with the parameter values listed in Table I, and then, the thickness of the separator is doubled, and the cell performance is predicted again. The result is shown in Table II. The predicted performances of Vaporvolt cells with different separator thicknesses are almost the same. This result indicates that the movement of the reaction layer in the cell has little effect on the performance of the cell. Therefore, the assumption that the electrochemical reaction occurs only at the surface of the active material is valid in this model.

Figure 2 shows the cell voltage change during the discharge with the parameter values listed in Table I, at various current densities. The cell voltage drops due to the increases in the overpotentials at the positive and the negative electrodes as we increase the current density during discharge. Therefore, the capacity and the energy density of the cell decrease with increasing current density of the cell during discharge, as shown in Fig. 3 and 4. However, the power density of the Vaporvolt cell is not a monotonic function of the current density. As shown in Fig. 5, the power density of the cell first increases and then decreases as the current density increases. So there exists a maximum power density value at a current density.

To determine the relative importance of the design feature of the cell (*e.g.*, thickness of the electrode) and the transport and kinetic parameters on the Vaporvolt cell's performance, a sensitivity analysis was done. The sensitivity analysis can indicate which parameters have the largest influence on the predicted performance of the Vaporvolt cell. If a small perturbation in a parameter does not change the predicted capacity significantly, energy density or the power density of the Vaporvolt cell, then that parameter could assume a large range of values, all of which give the same performance. The sensitivity coefficient can be defined as the dimensionless change in the predicted capacity, energy density, and the power density of the cell for a small dimensionless perturbation in a parameter j, while holding all other parameters constant[22]

$$\text{Sensitivity} = \frac{\partial G/G}{\partial \theta_j/\theta_j} \qquad [28]$$

where θ_j is the parameter and G is the capacity, the energy density, or the power density of the cell. Hence, large sensitivity coefficients mean that the parameter of interest significantly influences the cell performances. If the sensitivity coefficients for a parameter is large, the parameter should be obtained with more accuracy through further modeling or experimental studies. That is, if the value for a parameter is not known accurately and the parameter has

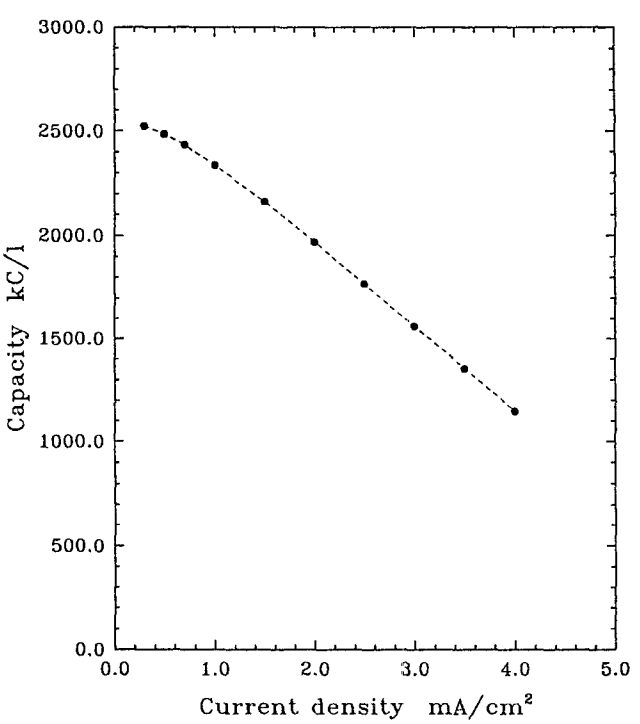

Fig. 3. The effects of current density on capacity of Vaporvolt cells.

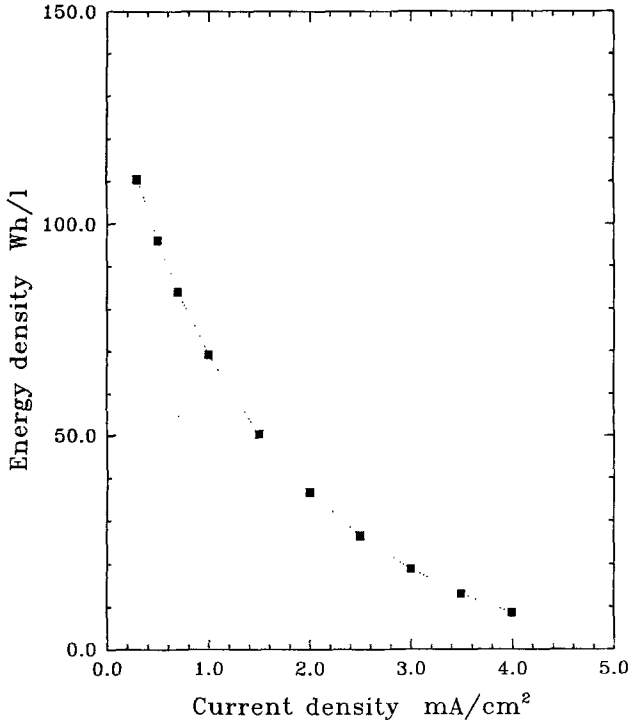

Fig. 4. The effects of current density on energy density of Vaporvolt cells.

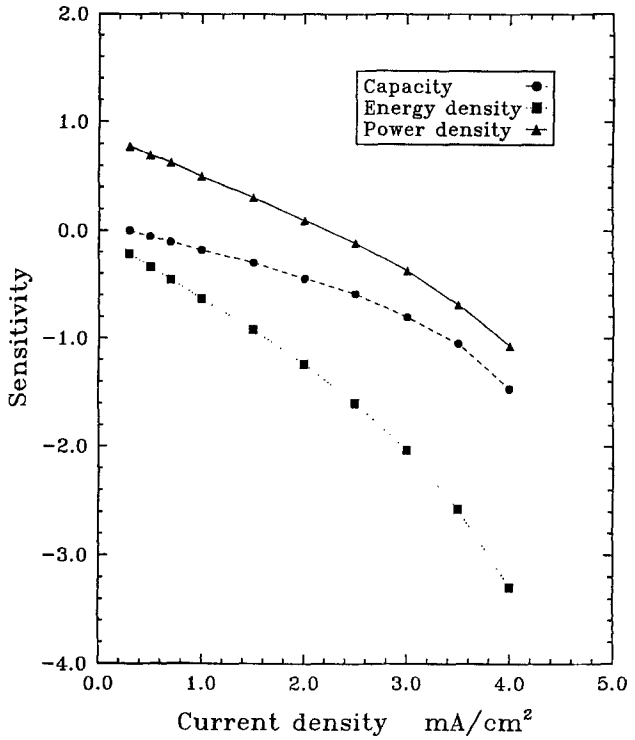

Fig. 6. Sensitivity of model predictions to the changes in current density.

a large sensitivity coefficient, then that parameter value should be ascertained more accurately to gain confidence in the model predictions.

All sensitivity coefficients calculated for this work were accomplished by increasing the value of the parameter of interest by 5% and calculating the resulting change in the capacity, energy density, and power density of the cell. For example, to get the sensitivity coefficient for the cell capacity on the separator thickness when the separator is 0.1 cm, the capacity was calculated at 0.1 cm and 0.105 cm and the sensitivity coefficient was calculated based on Eq. 28. The sensitivity coefficients for various parameters are shown in Fig. 6 through 10. As shown in Fig. 6, the model predictions are most sensitive to the current density.

The model predictions show little sensitivity to small perturbations in the KOH concentration as shown in Fig 7. This is because the IR drop due to the resistance of the electrolyte is negligible since the thickness of the separator is very small. The concentration of KOH in this region has very small effects on the capacity, energy density, and power density of the cell.

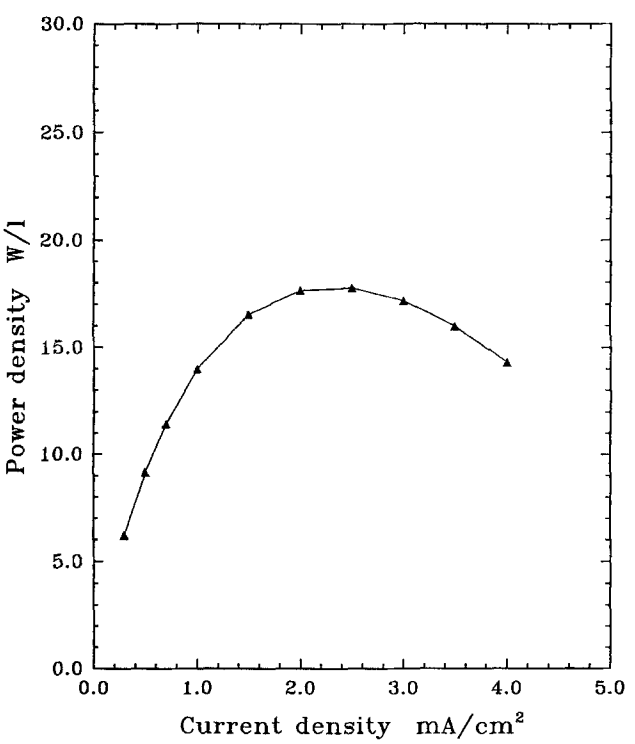

Fig. 5. The effects of current density on power density of Vaporvolt cells.

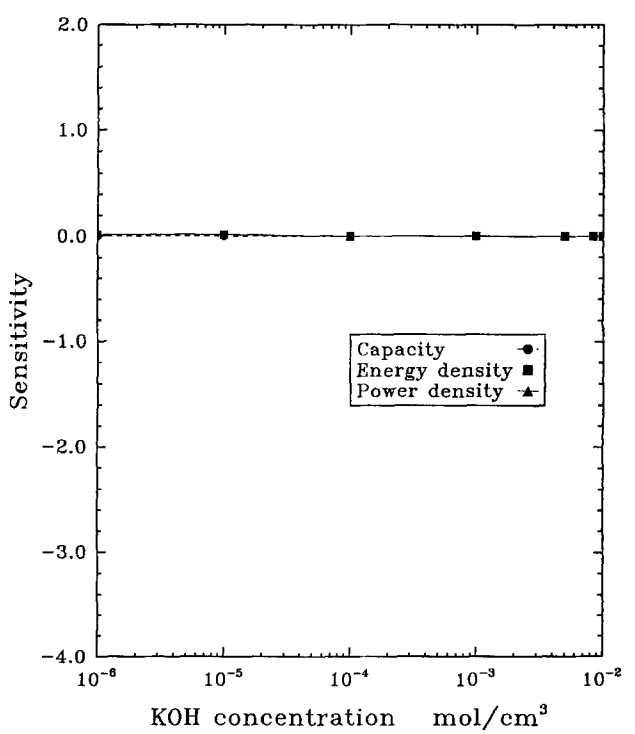

Fig. 7. Sensitivity of model predictions to changes in the concentration of KOH.

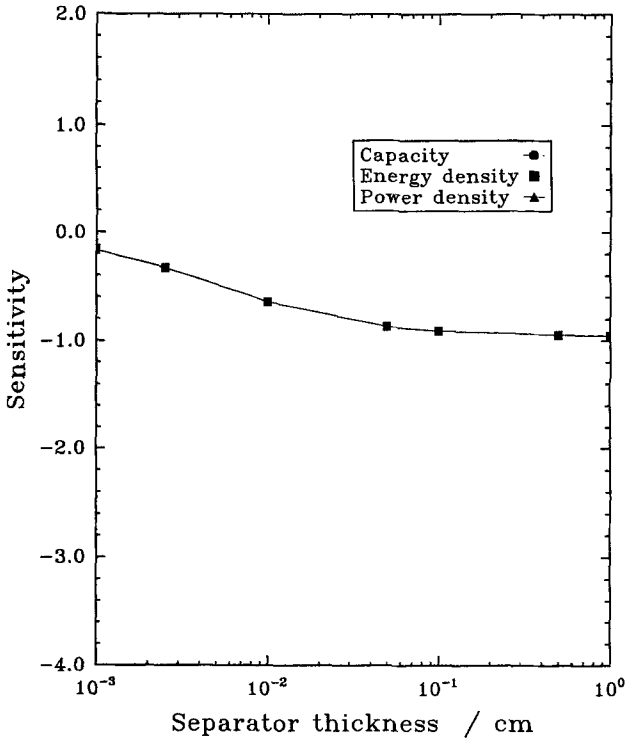

Fig. 8. Sensitivity of model predictions to changes in the thickness of the separator.

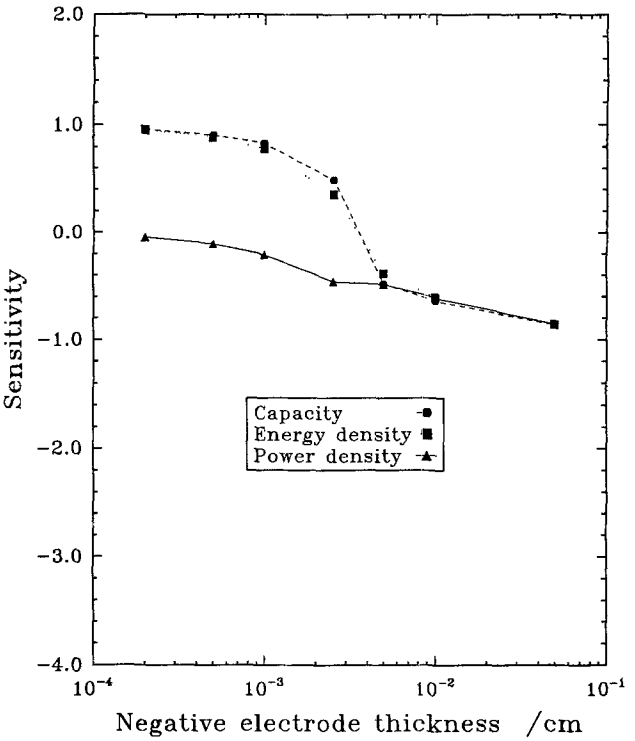

Fig. 10. Sensitivity of model predictions to changes in the thickness of the negative electrode.

The effects of the Vaporvolt cell separator thickness on the predicted performance are shown in Fig. 8. The sensitivity coefficients for the capacity, energy density, and power density of the cell decrease similarly and monotonically with the increase in separator thickness. Therefore, the separator should be as thin as possible. However, to avoid shortening the cell, the thickness of the separator should be about 0.001 cm.

Figures 9 and 10 show the effects of Vaporvolt cell positive and negative electrode thickness on predicted performances. The capacity and the energy density of the Vaporvolt cell increase as we increase the electrode thicknesses up to 0.002 cm since the sensitivity coefficients for the capacity and the energy density are positive in this region, but the capacity and the energy density decrease as we increase the electrode thicknesses when the thicknesses are above 0.002 cm. Therefore, the capacity and energy density become their maximum when electrode thicknesses are about 0.002 cm. The sensitivity coefficient for the power density of the cell is always negative, as shown in Fig. 9 and 10, so a small electrode thickness is favorable to get a larger power density. However; employing electrodes that are less than 0.001 cm could result in shortening the cell. A thickness of 0.001 cm is favorable for the positive and negative electrodes of a Vaporvolt cell to obtain maximum power density.

The maximum power density is obtained with a current density of 2.5 mA/cm^2 and 0.001 cm as the value for the thickness of the separator, and the positive and negative electrodes. As shown in Table III, the maximum power density obtained is 45.1 W/l; the capacity is 1768 kC/l and the

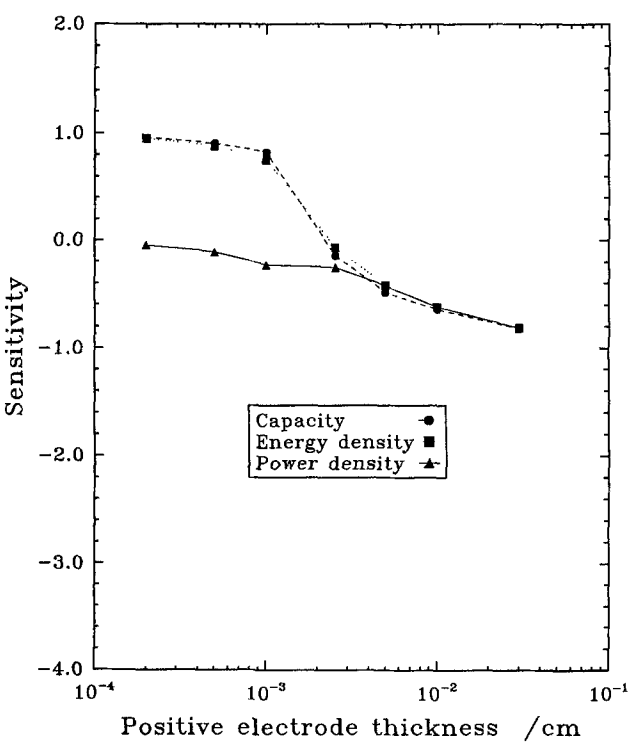

Fig. 9. Sensitivity of model predictions to changes in the thickness of the positive electrode.

Table III. Result of optimization.

Starting values	Optimized values
Current density = 0.001 A/cm^2	Current density = 0.0025 A/cm^2
Cell capacity = 2336 kC/l	Cell capacity = 1768 kC/l
Energy density = 69.1 Wh/l	Energy density = 26.5 Wh/l
Power density = 14.0 W/l	Power density = 45.1 W/l

Table IV. Comparison of the cell performances.

	CuO/Cu Vaporvolt	$Li/SOCl_2$	Li/MnO_2
Power density, W/l	45.1	80[a]	15[a]
Energy density, Wh/l	26.5	150[a]	50[a]
Unit cell open-circuit voltage, V	0.198	3.67[a]	3.5[a]

[a] These values are taken from Ref. 14.

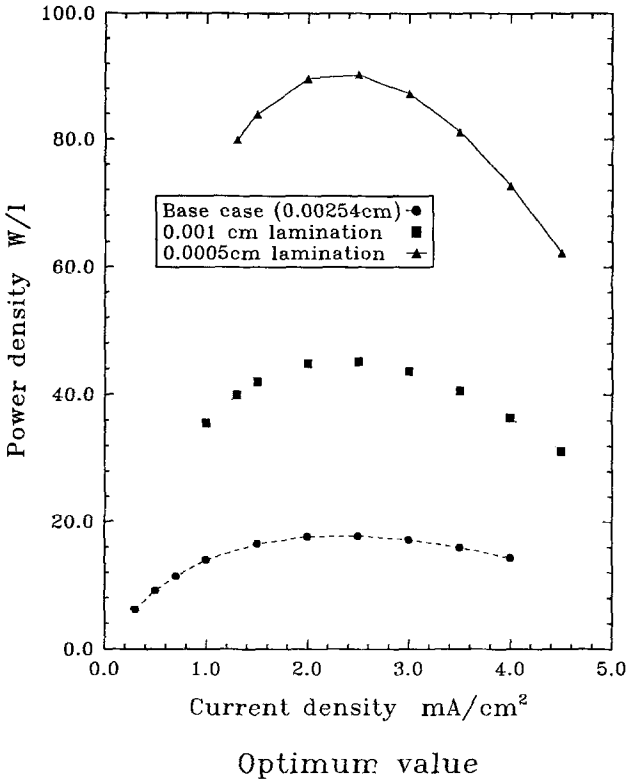

Fig. 11. The effects of current density on power density of the cell when thickness of the electrodes and of the separator are optimized.

energy density is 26.5 Wh/l at these parameter values. These values are lower than that of the high energy density primary cells, such as $Li/SOCl_2$ cells, which highest power density is approximately 80 W/l and its energy density is about 150 Wh/l when the highest power density is obtained,[14] however; the maximum attainable power density of a CuO/Cu Vaporvolt cell is much higher than that of Li/CF_x or Li/MnO_2 cells, which highest power density is approximately 15 W/l and the energy density is about 50 Wh/l when the highest power density is obtained. This is summarized in Table IV. If stable electrodes with thicknesses less than 0.001 cm without the possibility of shortening the cell could be developed in the future, much larger power densities could be obtained. For example, if we can make electrodes and separators with thicknesses of 0.0005 cm, the maximum power density is 90.3 W/l, as shown in Fig. 11, and the capacity and the energy density are 1768 kC/l and 26.5 Wh/l, respectively.

Summary

A mathematical model of a CuO/Cu Vaporvolt cell is presented to predict the potential and transport behavior of the cell during discharge. A sensitivity analysis of a CuO/Cu Vaporvolt cell model indicates that several parameters can influence the performance of the system significantly. In particular, current density influences the performance significantly. The effects of various design parameters have been investigated to determine if optimal values exist for the parameters. The model has shown that the thicknesses of the electrodes and separator, and current density can be optimized to give the maximum attainable power density. The model has also shown that greater power density can be achieved with thinner electrodes and separators.

Acknowledgment

This work was supported by NASA Lyndon B. Johnson Space Center. We thank Mr. E. Darcy and Mr. B. Bragg at NASA Lyndon B. Johnson Space Center.

Manuscript submitted May 22, 1992; revised manuscript received Aug. 14, 1992.

Texas A&M University assisted in meeting publication costs of this article.

LIST OF SYMBOLS

A^*	active surface area of the electrode, cm^2
A	surface area of the electrode, cm^2
c_i	concentration of species i, mol/cm^3
c_i^o	initial concentration of species i, mol/cm^3
c_i^r	reference concentration of species i, mol/cm^3
D_i	diffusion coefficient for species i, cm^2/s
d_j	density of electrode j, g/cm^3
E	electrode potential, V
F	Faraday's constant, 96,487 C/mol
G	capacity, energy density, or power density
$\mathbf{i}$	current density vector, A/cm^2
i	current density, A/cm^2
i^o	exchange current density, A/cm^2
L	thickness, cm
M_j	molecular weight of electrode j, g/mol
m	amount of active material at time t, g/cm^2
m^o	initial amount of active material, g/cm^2
n_j	number of electrons transferred in reaction j
$\mathbf{N}_i$	flux vector of species i, $mol/(cm^2\text{-s})$
P	power density, W/l
p_i	anodic reaction order for species i
q_i	cathodic reaction order for species i
R	gas constant, 8.3143 J/(mol-K) or 82.057 cm^3 atm/(mol-K)
R_i	production rate of species i, $mol/(cm^3\text{-s})$
s_i	stoichiometric coefficient of species i
T	temperature, K
U	open-circuit potential, V
u_i	mobility of species i, $mol\text{-}cm^2/(J\text{-s})$
$\mathbf{v}$	electrolyte velocity vector, cm/s
z_i	charge number of species i

Greek symbols

α_a	anodic transfer coefficient
α_c	cathodic transfer coefficient
κ	conductivity of a solution, S/cm
η	overpotential, V
Φ	solution phase potential, V
θ_j	parameter j

Superscripts and subscripts

a	anode
c	cathode
i	species i
j	reaction j or electrode j
neg	negative electrode
pos	positive electrode
r	reference condition
s	separator layer

REFERENCES

1. H. Kawamoto, *J. Appl. Electrochem.*, **21,** 409 (1991).
2. K. M. Abraham and D. M. Pasquariello, *This Journal,* **137,** 1189 (1990).
3. K. M. Abraham, M. W. Rupich, and J. E. Elliot, *Electrochim. Acta,* **30,** 1635 (1985).
4. K. M. Abraham and J. E. Elliot, *This Journal,* **131,** 2212 (1984).
5. Y. Sato, T. Nomura, H. Tanaka, and K. Kobayakawa, *ibid.,* **138,** L37 (1991).
6. K. Naoi, K. Ueyama, and T. Osaka, *ibid.,* **136,** 2444 (1989).
7. E. Plichta, S. Slane, M. Uchiyama, M. Salomon, D. Chua, W. B. Ebner, and H. W. Lin, *ibid.,* **136,** 1865 (1989).
8. A. N. Dey, W. L. Bowden, H. C. Kuo, M. L. Gopikanth, C. Schlaikjer, and D. Foster, *ibid.,* **136,** 1618 (1989).
9. D. L. Thomas and D. Bennion, *ibid.,* **136,** 3558 (1989).
10. W. L. Bowden, L. H. Barnette, and D. L. DeMuth, *ibid.,* **136,** 1614 (1989).
11. E. Peled, Y. Sternberg, A. Gorenshtein, and Y. Lavi, *ibid.,* **136,** 1621 (1989).
12. J-F. Equey, S. Muller, and A. Tsukada, *J. Appl. Electrochem.,* **19,** 65 (1989).
13. J-F. Equey, S. Muller, and A. Tsukada, *ibid.,* **19,** 147 (1989).
14. J. P. Gabano, *Lithium Batteries,* p. 11, Academic Press Inc., New York (1983).
15. H. A. Kiehne, *Battery Technology Handbook,* p. 394, Marcel Dekker Inc., New York (1989).
16. Y. I. Cho and D. W. Chee, *This Journal,* **138,** 927 (1991).

17. T. I. Evans, T. V. Nguyen, and R. E. White, *ibid.*, **136,** 328 (1989).
18. S. R. Jones and T. Ichniowski, *Chemical Week*, **138,** 11, (1986).
19. M. C. Gourdine, Final Report to NASA Lyndon B. Johnson Space Center, Contract No. NAS9-17925 (1988).
20. M. Pourbaix, *Atlas of Electrochemical Equilibria in Aqueous Solutions,* p. 384, Pergamon Press, Ltd., New York (1966).
21. J. S. Newman, *Electrochemical Systems,* p. 241, Prentice Hall, Inc., Englewood Cliffs, NJ (1991).
22. D. K. Anand, *Introduction to Control Systems,* p. 165, Pergamon Press, Ltd., New York (1984).

Investigation of Photocatalytic Decomposition Mechanism of Organic Compounds on Platinized Semiconductor Catalyst by Rotating Ring Disk Electrode Technique

Gyoichi Nagomi

Department of Electrical Engineering, Kyushu Institute of Technology, Tobata-ku, Kitakyushu 804, Japan

ABSTRACT

Rotating Pt-ring TiO_2-disk electrodes were used to investigate the catalytic mechanism of Pt sites in platinized semiconductor catalysts. When a TiO_2 disk electrode immersed in a methanol-water mixture was illuminated with chopped light, an anodic current was observed at the Pt ring electrode even at cathodic potentials at which reduction (cathodic) current was expected to flow. This peculiar phenomenon was enhanced by oxygen bubbling and could be observed only in solutions with pH < 8. The phenomenon was analyzed in terms of a $HO_2^{\bullet}$ radical which can promote a deprotonation reaction of organic compounds such as methanol. The decomposition (oxidation) of organic compounds also can occur at Pt sites in the presence of oxygen and hydrogen ions.

Semiconductor photocatalysts are theoretically and practically important in using solar energy to synthesize new chemical products and fuels from chemical materials and/or biomass.[1-21] Platinized titanium dioxide powder was applied successfully to photoelectrosynthesize ethane from acetate ions (the photo-Kolbe reaction)[3] and amino acids from a methane-ammonia-water mixture.[5]

Photocatalytic production of hydrogen from various biomass sources such as wood, cotton, etc., also has been demonstrated over Pt-TiO_2/water suspensions.[7,13-15]

The following experimental results are well known: (*i*) the deposition of platinum on a semiconductor greatly enhances its catalytic activity.[4,8,10-16] Platinum promotes electron transfer from the semiconductor to redox species in solution and then reduces the possibility of recombination between electrons and holes; (*ii*) the catalytic decomposition of organic compounds simultaneously with photosynthetic hydrogen evolution requires the presence of water.[2] A hydroxyl radical, the product of water oxidation, may be an intermediate which plays the decisive role in the photosynthetic activity of the system;[1,2] (*iii*) the decomposition rate of organic compounds by photocatalysts is greatly enhanced when oxygen is bubbled into the organic-water mixture.[8,19]

However, due to the fundamental disadvantage of the catalytic particulate system in which oxidation and reduction sites cannot be separated spacially from each other, the detailed mechanism of photodecomposition remains unknown.

Macroelectrode systems have the advantage of allowing spacial separation of the anodic and cathodic reaction sites.[20] Moreover, if a rotating platinum-ring TiO_2-disk electrode (RRDE) is used, kinetic parameters and the detailed mechanism associated with electrode processes may be clarified because of this electrode's hydrodynamics.

To elucidate the decomposition mechanism of organic compounds, we have found a phenomenon where the net ring current responding to the disk current is anodic in methanol-containing solutions even when the Pt ring is cathodically biased.

Experimental

The system used was the same as described elsewhere.[24] A c-cut wafer of a single crystal TiO_2 purchased from Furuuchi Chemical Co., was used to prepare the TiO_2 disks. Sample preparation conditions were reported previously.[22] A disk electrode with a diameter of 0.6 cm, and a Pt ring electrode with an inner diameter of 0.7 cm and an outer diameter of 0.92 cm were used. The calculated collection efficiency N_0 was 0.39. The doping concentrations of the TiO_2 disks estimated from the Mott-Schottky plots at 1 kHz ranged from $1 \times 10^{17} \sim 5 \times 10^{17}$ cm^{-3}. The supporting electrolyte was $0.1M$ Na_2SO_4. The pH was adjusted in individual experiments by adding H_2SO_4 or NaOH. The solutions were purged with nitrogen for at least 10 min before each measurement.

Results

Figure 1 shows typical current-potential curves under chopped light illumination, with and without CH_3OH at a chopping frequency of *ca.* 0.25 Hz. The measured pHs were 3.01 and 3.45, respectively. Before addition of CH_3OH, the light intensity was adjusted to give a disk current of 500 μA at 1.0 V *vs.* SCE. This current is due to the oxidation of water. Thirty volume percent (v/o) CH_3OH was added without changing other experimental conditions. The anodic disk current increased from 500 μA when methanol was added because methanol is a "current-doubling" agent. In Fig. 1, I_D increased from 500 to 640 μA. The increment of disk current due to the current-doubling effect of methanol depended on the past history of the TiO_2 disk used. In both solutions, the disk current I_D was slightly anodic with the light off in a potential range from 0 to 1.0 V *vs.* SCE. For example, the dark disk current was about 5 μA at 1.0 V *vs.* SCE. The ring current was recorded as a function of ring potential. As apparent from the upper part in Fig. 1, a plateau region could be observed near −1.0 V *vs.* SCE for both solutions. The potential region where this current is observed indicates that this plateau can be attributed to oxygen and hydrogen ion reduction.[24] In addition, the ring current at the plateau increases when additional hydrogen ions are supplied from the disk due to deprotonation reaction at the illuminated TiO_2 disk: ($2H_2O + 4H^+$ (VB) $\rightarrow O_2 + 4H^+$), although this is not shown in Fig. 1. The lifetime of hydrogen ions thus formed is expected to be relatively long in acidic and neutral solutions and can be detected at the ring electrode.[24] On the contrary, it cannot be detected in basic solutions due to rapid recombination with OH^- ($H^+ +$